Published in IET Microwaves, Antennas & Propagation
Received on 18th March 2010
doi: 10.1049/iet-map.2010.0111

ISSN 1751-8725

Optimisation of a microstrip left-handed transmission line using circuit modelling

A. Levy[1] *R. Shavit*[1] *L. Habib*[2]

[1]*Department of Electrical and Computer Engineering, Ben-Gurion University of the Negev, Beer Sheva 84105, Israel*
[2]*Elta Electronic Industries Ltd., Ashdod 77102, Israel*
E-mail: rshavit@ee.bgu.ac.il

Abstract: Two circuit modelling and parameterisation techniques for optimisation of a left-handed microstrip transmission line for antenna applications are presented. Such a transmission line is characterised by high transmission loss ripples in the required frequency band, which hinders its use as a wideband feeding network in antenna array applications. The first circuit modelling technique is based on numerical parameterisation, whereas the second is based on analytical parameterisation. The goal of the parameterisation is to obtain multivariable functions to represent the components of the circuit model with the geometrical dimensions as parameters. A novel and improved circuit model taking into consideration the external mutual coupling between the elements of the left handed transmission line was used to optimise its performance in terms of absolute transmission loss and minimum ripple over a wide frequency band. The performance of the improved equivalent circuit model is compared with the electromagnetic simulations, and a good agreement is obtained. A prototype of the optimised left-handed transmission line was built and tested. Satisfactory agreement was obtained between the simulated and measurement results.

1 Introduction

In recent years, the amount of research on metamaterials, in particular on metamaterials that exhibit double negative characteristics, has increased significantly. In many cases, this research focuses on antenna applications. One important application of double negative materials is their use as transmission lines. Such a transmission line is called a left-hand transmission line (LHTL) because its electromagnetic (EM) fields and the propagation vector observe the left-hand rule in contrast to a standard transmission line, which is called right-hand transmission line (RHTL) and for which the right-hand rule is observed. In the LHTL, the phase accumulation along the line is positive, whereas the phase accumulation along an RHTL is negative. Thus, for instance, a combination of an LHTL and RHTL connected in tandem can be used to generate low loss with zero phase accumulation between two interconnected antenna elements. This effect can be used in a serial fed array without the need to use long meandered lines, which may also cause undesirable parasitic radiation. It is well known that a shunt capacitor and a serial inductor can represent the equivalent circuit of an incremental RHTL. Similarly, a shunt inductor and a serial capacitor can represent an incremental LHTL. Two different methods have been proposed to implement an LHTL using microstrip technology. The first method proposed by Gil *et al.* [1] is based on the complementary split ring resonator element, in which a slot ring is cut in the ground plane. This implementation exhibits severe ripples in the transmission loss as a function of frequency and therefore is not suitable for broadband microwave and antenna applications as discussed in [2]. The second approach proposed by Caloz and Itoh [3, 4] and adopted in this work is based on a combination of interdigitated capacitors and shunt stub inductors. This approach exhibits a larger bandwidth in comparison with the first approach, but the transmission loss ripples in the range of interest are still present.

This paper presents an effective method for optimisation of the transmission loss performance using circuit modelling. The objective of the circuit modelling is to obtain for each component in the equivalent circuit a

multivariable function with the physical dimensions of the LHTL as its variables. The circuit modelling and the parameterisation are obtained by two methods. The first method is based on the circuit model proposed by Caloz and Itoh [3] and is followed by a numerical l_1 optimisation technique described by Bandler *et al.* [5]. The second method is based on integration of low-geometrical level circuit models of the LHTL with analytical parameterisation functions. A novel and improved circuit model taking into consideration the external mutual coupling between the elements of the left-handed transmission line was used to optimise its performance in terms of absolute transmission loss and minimum ripple over a wide frequency band. In the final phase of the design process, the optimised equivalent circuit components values are converted into physical dimensions of the LHTL and the EM transmission loss performance is compared to the transmission loss of the equivalent circuit. A prototype of the optimised LHTL was built and tested. Comparison between the simulated and the measurement results is presented.

2 Circuit modelling

The LHTL under investigation is made of unit cells with each unit cell consisting of a shunt stub inductor implemented by a shorted stub via at its end and a series capacitor implemented by an interdigitated capacitor, as shown in Fig. 1. The equivalent circuit of the unit cell is shown in Fig. 2. The equivalent circuit of an interdigitated capacitor is a π-network [3] as shown in Fig. 2*a*, while a T-network [3] as shown in Fig. 2*b* represents the shunt stub inductor.

The equivalent circuit components of the interdigitated capacitor are (C_P^{ic}, L_S^{ic},C_S^{ic}) in which C_P^{ic} represents the interdigitated capacitor capacitance to the ground, C_S^{ic} represents the mutual coupling capacitance between the interdigitated capacitor fingers and L_S^{ic} represents the inductance of the interdigitated capacitor fingers. The equivalent circuit components of the shunt stub inductor are (C_P^{si}, L_P^{si}, L_S^{si}) in which C_P^{si} represents the shorted stub capacitance, L_P^{si} represents the shorting via inductance and

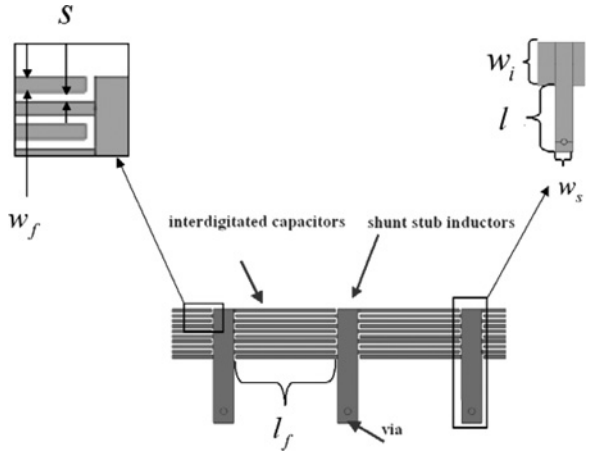

Figure 1 *Unit cell of the LHTL described in [3, 4] made of a series interdigitated capacitor and a shorted shunt stub with a via*

L_S^{si} represents the serial inductance at the junction. The equivalent circuit for the combined interdigitated capacitor and shunt stub inductor unit cell is shown in Fig. 2*c*. This equivalent circuit holds for small unit cell sizes (less than $\lambda/10$).

Our objective is to obtain for each component in the equivalent circuit a multivariable function with the physical dimensions as its variables. This can be accomplished by a numerical parameterisation technique or by integration of low-geometrical level circuit models with analytical parameterisation functions.

2.1 Numerical parameterisation technique

The numerical parameterisation technique adopted in this study is an iterative technique, which compiles a multivariable function for each component in the equivalent circuit. These functions relate the circuit components values to the physical dimensions of the layout as shown in Fig. 1. This technique requires a priori knowledge of the equivalent circuit, which is available in our case based on physical insight as shown in Fig. 2. Conceptually, the technique applied in this study follows

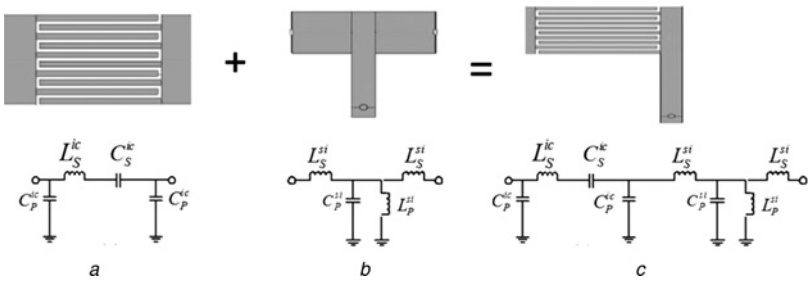

Figure 2 *Equivalent circuit of the LHTL based on [3]*

a Interdigitated capacitor
b Shunt stub inductor
c Combined interdigitated capacitor and shunt stub inductor in a LHTL unit cell

doi: 10.1049/iet-map.2010.0111

the technique described in [5]. The relevant components in the equivalent circuit are C_P^{ic}, L_S^{ic}, C_S^{ic} for the interdigitated capacitor and C_P^{si}, L_P^{si}, L_S^{si} for the shunt stub inductor. The relevant physical dimensions for the interdigitated capacitor are N-number of fingers on each side of the microstrip, w_f, s, l_f and for the shunt stub inductor are w_i, l and w_s (see Fig. 1). Initially, a data bank of the EM scattering parameters, S_{11}^{EM} and S_{21}^{EM} in the relevant frequency range and for different physical dimensions is established. The increment in the physical dimensions is chosen to be approximately 10–20% of the initial value. In this study, the EM scattering parameters were computed using the commercial EM simulator momentum of advanced design systems (ADS) from Agilent, which is especially effective for printed multilayer circuits. The data bank is collected separately for the interdigitated capacitor and for the shunt stub inductor to reduce as much as possible accumulative errors in the equivalent circuit. The next step would be to determine the best fit between the equivalent circuit scattering parameters, S_{11}^{ckt}, S_{21}^{ckt} computed by the commercial software ADS from Agilent to the EM scattering parameters, S_{11}^{EM}, S_{21}^{EM} over the entire frequency band. The value of the circuit components is obtained throughout an iterative process, which minimises the error function (E) given by

$$E = \frac{1}{2K}\sum_{i=1}^{K}[|S_{11}^{EM} - S_{11}^{ckt}| + |S_{21}^{EM} - S_{21}^{ckt}|]^2 \qquad (1)$$

in which K denotes the number of sampled frequencies in the band. The initial values of the components in the equivalent circuit are computed at the LHTL centre band frequency ω_e, using the relationships between the admittance parameters Y_{11} and Y_{21} of the π-network in Fig. 2*a* vis-à-vis the components C_P^{ic}, L_S^{ic}, C_S^{ic} and the impedance parameters Z_{11} and Z_{21} of the T-network in Fig. 2*b* vis-à-vis the components C_P^{si}, L_P^{si}, L_S^{si}. Both the admittance and impedance values can be computed from the scattering matrix [$\boldsymbol{S}$] as described in [3]. It can be easily shown that the interdigitated capacitor components can be computed by

$$C_S^{ic} = \left(\frac{\mathrm{Im}\{Y_{12}\}}{\omega_e}\right)\left(\frac{\omega_e^2}{\omega_{ic}^2} - 1\right), \quad C_P^{ic} = \frac{\mathrm{Im}\{Y_{11} + Y_{12}\}}{\omega_e}$$
$$\text{and} \quad L_S^{ic} = \frac{1}{\omega_{ic}^2 C_S^{ic}} \qquad (2)$$

in which ω_{ic} is the resonant frequency satisfying the condition $\mathrm{Im}\{Y_{12}\} = 0$. Similarly, the initial values of the components of the shunt stub inductor can be computed by

$$L_P^{si} = \frac{\mathrm{Im}\{Z_{12}\}}{\omega_e}\left(1 - \frac{\omega_e^2}{\omega_{si}^2}\right), \quad L_S^{si} = \frac{\mathrm{Im}\{Z_{12} - Z_{11}\}}{\omega_e}$$
$$\text{and} \quad C_P^{si} = \frac{1}{\omega_{si}^2 L_P^{si}} \qquad (3)$$

in which ω_{si} is the resonant frequency satisfying the condition $\mathrm{Im}\{Z_{12}\} = 0$.

Once the components values are obtained at the tested discrete physical dimensions, a polynomial fit procedure is applied to obtain the multivariable functions of the components $C_P^{ic}(N, w_f, s)$, $L_S^{ic}(N, w_f, s)$, $C_S^{ic}(N, w_f, s)$ for the interdigitated capacitor and $C_P^{si}(w_i, l)$, $L_P^{si}(w_i, l)$ and $L_S^{si}(w_i)$ for the shunt stub inductor. Usually, first or second-order polynomial fit would be sufficient. These multivariable functions are used in a later section for the optimisation procedure to obtain smooth transmission loss and good matching over a wide bandwidth of the LHTL.

2.2 Physical parameterisation technique

The major drawback of the numerical parameterisation technique is the need for a priori knowledge of the equivalent circuit structure as shown in Fig. 2. On the other hand, the physical parameterisation technique outlined in this section generates the equivalent circuit structure by considering the device as an assembly of more primitive structures with known equivalent circuits. These low-geometrical level circuits have analytical parameterisation functions. The integration of the simple equivalent circuits is done by using physical considerations. Although the equivalent circuit in our specific case is known (i.e. Fig. 2), it will be shown how it can be obtained for both the interdigitated capacitor and the shunt stub inductor substructures to demonstrate the technique. A major advantage of the technique is in obtaining analytical rather than numerical multivariable functions for the components in the equivalent circuit, a fact that speed up the computation time.

In the interdigitated capacitor equivalent circuit shown in Fig. 2*a*, the capacitor C_P^{ic} can be approximated by the capacitance of a short microstrip line with width, w_i and length l_f. Based on the transmission line theory, $C_P^{ic} = (1/2)(l_f\sqrt{\varepsilon_{e1}}/cZ_{e1})$ in which ε_{e1} and Z_{e1} are, respectively, the effective dielectric constant and the characteristic impedance of the microstrip line [6] and c is the speed of light in free space. Fig. 3 shows a sketch of the interdigitated capacitor and the various contributors to its equivalent circuit. One can observe that the interdigitated capacitor is made of N coplanar strip lines of length l_f ($l_f \ll \lambda$,) connected in parallel. The contributors to the serial capacitor C_S^{ic} are the capacitance C of N coplanar strip lines with length l_f and width w_f, the gap capacitance C_{ge} between the strip fingers and the microstrip line with width w_i and the mutual coupling capacitance C_f between the coplanar strip lines. Thus, $C_S^{ic} = NC + C_{ge} + (N-1)C_f$. The capacitance of each coplanar strip line can be computed by $C = l_f(\sqrt{\varepsilon_{e2}}/cZ_{e2})$ in which ε_{e2} and Z_{e2} are the effective dielectric constant and the characteristic impedance of the coplanar strip line described in [7]. The computation of the gap capacitance C_{ge} is described

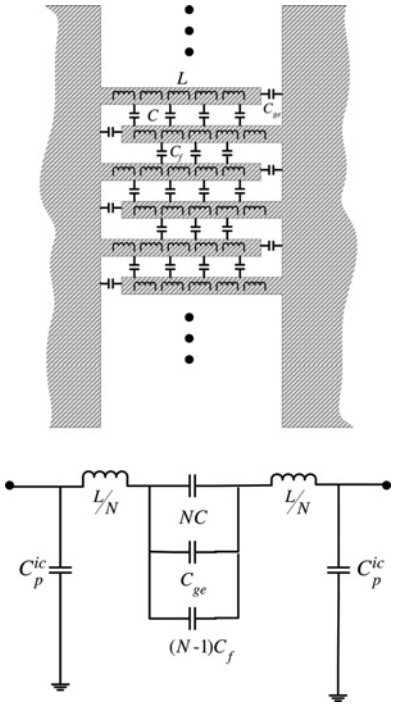

Figure 3 *Equivalent circuit of the interdigitated capacitor and its various components*

in [8] and is given by

$$C_{ge} = \frac{w_i}{2}\left(C_{odd} - \frac{1}{2}C_{even}\right) \tag{4}$$

in which a polynomial fit of Fig. 7*a* in [8] yields $C_{odd} = 42.246(s/w_i)^{-0.2775}$ and $C_{even} = -8.7474(s/w_i)^2 + 33.917(s/w_i) - 0.1224$. The mutual coupling capacitance, C_f, between adjacent coplanar strip lines can be approximated by the fringing capacitance of the coplanar strip line discussed in [9] and which is given by

$$C_f = \frac{l_f C_f' \sqrt{\varepsilon_r/\varepsilon_{e2}}}{1+\exp[-0.1(\exp(2.33-2.53(w_f/h)))](h/s)\tanh(10s/h)} \tag{5}$$

in which $C_f' = 0.5(\sqrt{\varepsilon_{e2}}/cZ_{e2}) - \varepsilon_0\varepsilon_r(w_f/h))$ and ε_{e2}, Z_{e2} are, respectively, the effective dielectric and characteristic impedance parameters of the coplanar strips with dimensions w_f and s. The inductance, L_S^{ic}, of the interdigitated capacitor shown in Fig. 2, can be computed as an assembly of N parallel-connected inductances (i.e. Fig. 3) related to the number of coplanar strip lines. Actually, each parallel inductance is composed of two serial inductances, L equal to the inductance of a short microstrip line with width w_f and length l_f. This results in $L_s^{ic} = 2L/N$ with $L = l_f Z_{e3}\sqrt{\varepsilon_{e3}}/c$ in which ε_{e3} and Z_{e3} are the effective dielectric constant and the characteristic impedance of a microstrip line [6] with width w_f and length l_f printed on a substrate with thickness h.

Fig. 4 shows a sketch of the shunt stub inductor and the proposed assembly of its equivalent circuit. Two microstrip lines combine at the junction, one characterised by the parameters ε_{e1}, Z_{e1}, w_i and the other by ε_{e2}, Z_{e2}, w_s representing the effective dielectric constant, the characteristic impedance and the width, respectively. The short microstrip line between the reference lines T_1 and T_2 with width w_i and length $w_s/2 - d_1$ can be represented as a combination of a serial inductor, $L_s = ((w_s/2) - d_1)(\sqrt{\varepsilon_{e1}}Z_{e1}/c)$ and a shunt capacitance $C_s = ((w_s/d) - d_1)(\sqrt{\varepsilon_{e1}}/Z_{e1}c)$ in which c is the speed of light in free space. The parallel junction capacitance C_T is derived in [10, 11] and reproduced here

$$C_T = \begin{cases} \dfrac{w_{e1}}{\omega\lambda_1 Z_{e2}}\left(1-2\dfrac{w_{e1}}{\lambda_1}\right) & \text{for } Z_{e1} \le 0.5Z_{e2} \\ \dfrac{w_{e1}}{\omega\lambda_1 Z_{e1}}\left(2-3\dfrac{Z_{e1}}{Z_{e2}}\right)\left(1-2\dfrac{w_{e1}}{\lambda_1}\right) & \text{for } Z_{e1} \ge 0.5Z_{e2} \end{cases} \tag{6}$$

in which $\lambda_1 = \lambda_0/\sqrt{\varepsilon_{e1}}$, $w_{e1} = 120\pi h/Z_{e1}\sqrt{\varepsilon_{e1}}$ and $w_{e2} = 120\pi h/Z_{e2}\sqrt{\varepsilon_{e2}}$. The transformation from the microstrip line Z_{e1} to Z_{e2} until the reference line T_3 can be represented by a transformer n:1 [10, 11] with $n = \sin(x)/x$;

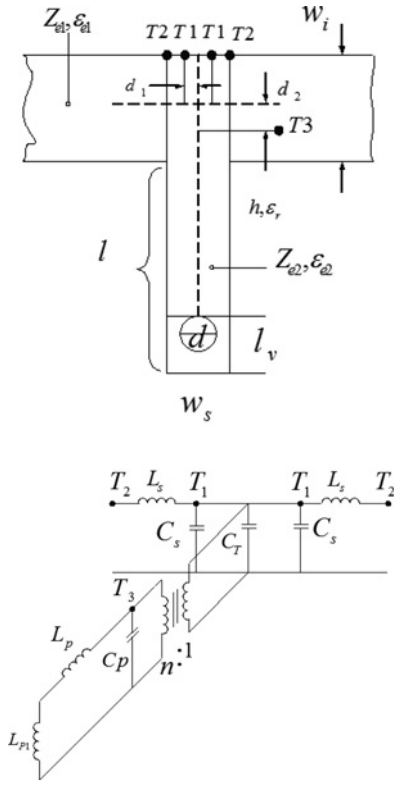

Figure 4 *Shunt stub inductor and the proposed assembly of its equivalent circuit*

doi: 10.1049/iet-map.2010.0111

$x = (\pi/2)(2w_{e1}/\lambda_1)(Z_{e1}/Z_{e2})$. The short microstrip line from the reference line T_3 until the stub's via has a length of $l' = l - l_v + ((w_i/2) - d_2)$ and can be represented by a series inductance $L_p = l'(\sqrt{\varepsilon_{e2}} Z_{e2}/c)$ and a shunt capacitance $C_p = l'(\sqrt{\varepsilon_{e2}}/Z_{e2}c)$. The lengths d_1 and d_2 are computed in [11, 12] and are equal to

$$d_1 = \frac{0.05 w_{e2} n^2 Z_{e1}}{Z_{e2}} \tag{7}$$

with

$$d_2 = 0.5w_{e1} - w_{e1}\left(\frac{Z_{e1}}{Z_{e2}}\right)\left\{0.076 + 0.2\left(2\frac{w_{e1}}{\lambda_1}\right)^2 \ldots + 0.663\exp\left(-\frac{1.71 Z_{e1}}{Z_{e2}}\right) - 0.172\ln\left(\frac{Z_{e1}}{Z_{e2}}\right)\right\} \tag{8}$$

Finally, the via with diameter d can be represented by an inductance L_{p1}, which has been computed in [13] and equals to

$$L_{p1} = \frac{60h}{c}\ln\frac{4}{\gamma k\sqrt{\varepsilon_r} d} \tag{9}$$

in which $\gamma = 1.781$, $k = 2\pi/\lambda_0$ and c is the speed of light in free space. Combining the components shown in Fig. 4, results in the equivalent circuit of the shunt stub inductor shown in Fig. 2*b*, such that $L_S^{si} = L_s$, $C_P^{si} = C_T + 2C_s + C_p n^2$ and $L_P^{si} = (L_p + L_{p1})/n^2$.

The geometry described in [4] has been considered as a test case, and the circuit modelling technique outlined above was applied to generate the multivariable functions of the interdigitated capacitor and shunt stub inductor equivalent circuits. The interdigitated capacitor and shunt stub inductor were printed on a dielectric substrate with height $h = 1.57$ mm and electrical properties $\varepsilon_r = 2.2$, $\tan\delta = 0.0009$. Fig. 5 shows a comparison between the equivalent circuit interdigitated capacitor components C_P^{ic}, L_S^{ic}, C_S^{ic} computed by the numerical technique described above and by the physical parameterisation technique as a function of the geometrical parameters w_f and s for $N = 5$. All three parameters, C_P^{ic}, L_S^{ic}, C_S^{ic} have been polynomial fitted by a third-order polynomial $X(N, s, w_f) = a_3^{ic}(N, s)w_f^3 + a_2^{ic}(N, s)w_f^2 + a_1^{ic}(N, s)w_f + a_0^{ic}(N, s)$ in which $X = C_P^{ic}$, L_S^{ic} or C_S^{ic}. The set of coefficients $a_0^{ic}(N, s)$, $a_1^{ic}(N, s)$, $a_2^{ic}(N, s)$ and $a_3^{ic}(N, s)$ are uniquely determined for the interdigitated capacitors in the equivalent circuit. Fig. 6 shows the comparison between the equivalent circuit shunt stub inductor components C_P^{si}, L_P^{si}, L_S^{si} computed by the numerical technique described above and by the physical parameterisation technique, as a function of the geometrical parameters l and w_i with $w_s = 2$ mm. One can observe a nice agreement between the results computed by the two

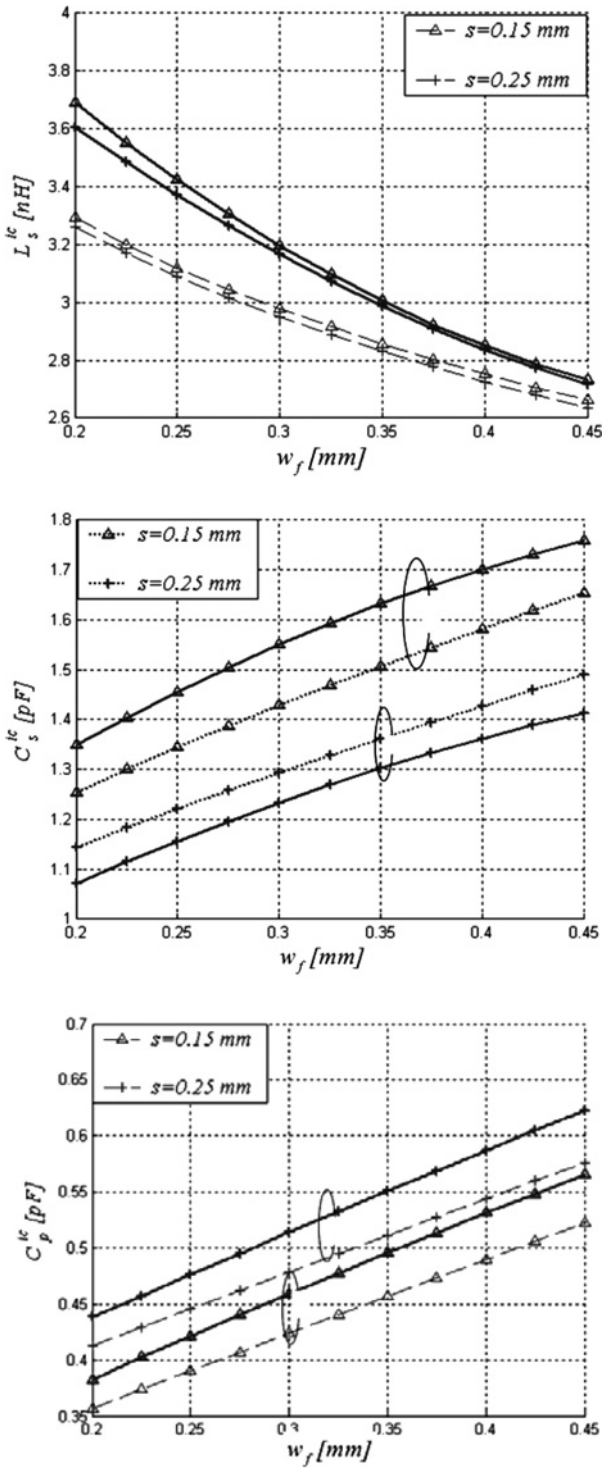

Figure 5 *Comparison between the components $L_S^{ic}(N, w_f, s)$, $C_S^{is}(N, w_f, s)$, $C_P^{ic}(N, w_f, s)$ values computed by the numerical technique (solid lines) and the physical parameterisation technique (dashed lines) as a function of the geometrical parameters w_f and s for $N = 5$*

methods. The stub inductor parameters C_P^{si} and L_P^{si} have been polynomially fitted by a linear approximation $\Psi(w_i, l) = a_1^{si}(w_i)l + a_0^{si}(w_i)$, in which $\Psi = C_P^{si}$ or L_P^{si} and $L_s^{si}(w_i) = c_1^{si}w_i + c_0^{si}$. The set of coefficients $a_0^{si}(w_i)$,

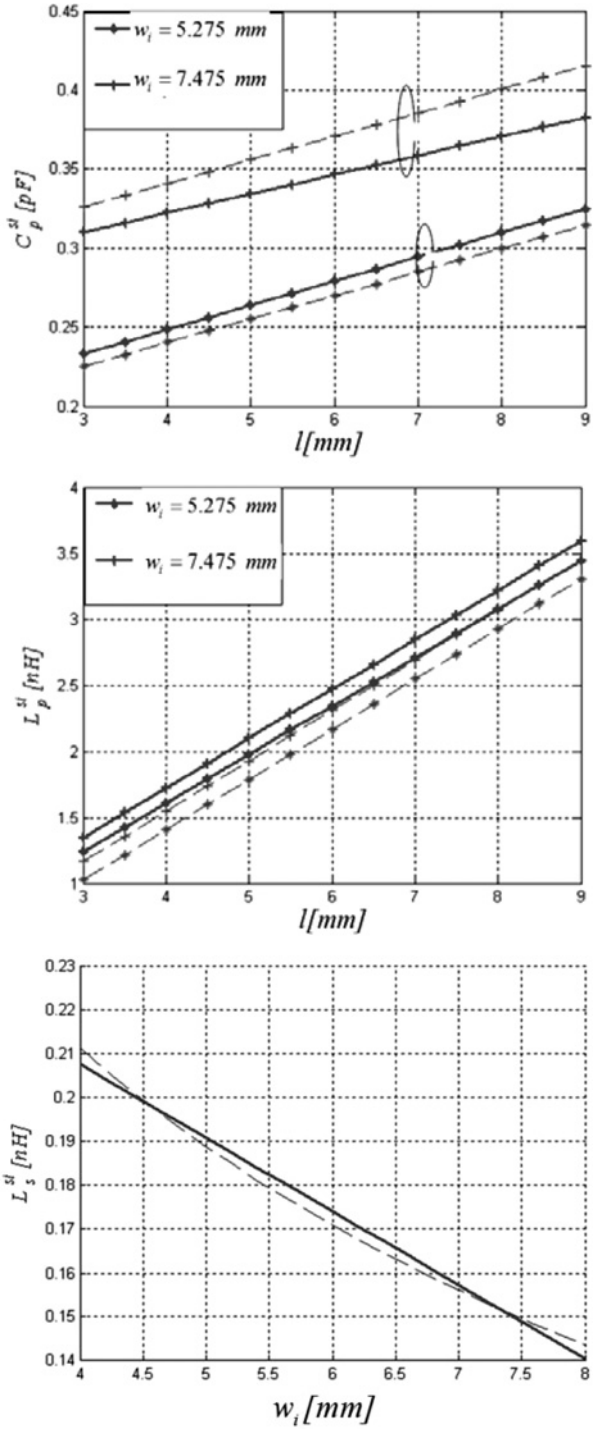

Figure 6 *Comparison between the components $C_P^{si}(w_i, l)$, $L_P^{si}(w_i, l)$, $L_S^{si}(w_i)$ values computed by the numerical technique (solid lines) and the physical parameterisation technique (dashed lines) as a function of the geometrical parameters l and w_i ($N = 5$ for $w_i = 5.275$ mm and $N = 7$ for $w_i = 7.475$ mm, also $w_s = 2$ mm)*

$a_1^{si}(w_i)$, c_0^{si} and c_1^{si} are uniquely determined for each of the stub inductor equivalent circuit components, C_P^{si}, L_P^{si}, L_S^{si}. The set of functions $X(N, s, w_f)$ and $\Psi(w_i, l)$ have been used throughout the optimisation process of the LHTL.

3 Optimisation

As a test case to check the optimisation efficiency of the LHTL design using the circuit modelling functions developed in the previous section, an LHTL with seven unit cells was considered. The numerical parameterisation technique was used for the optimisation. For this purpose, the numerical multivariable functions were prepared as discussed in the previous section. The design goal of the optimisation process was a good match (return loss lower than 15 dB in the frequency band 1.4–2 GHz) and a low (less than 0.5 dB) and smooth (less than ± 0.1 dB) transmission loss over the frequency band (1.4–2 GHz). The initial geometrical dimensions are identical to these described in [3, 4] such that for $f < 2.3$ GHz the device operates as an LHTL. The optimisation process was performed by varying the physical parameters (N, s, w_f) related to the equivalent circuit components (C_P^{ic}, L_S^{ic}, C_S^{ic}) of the interdigitated capacitors and the physical parameters (w_i, l), in which $w_i = 2Nw_f + S(2N-1)$ related to the equivalent circuit components (C_P^{si}, L_P^{si}, L_S^{si}) of the shunt stub inductors. Direct optimisation of all equivalent circuit components proved to be time consuming with unsatisfactory results. Accordingly, the transmission line geometry was divided into two parts: the internal elements comprise six interdigitated capacitors and seven shunt stub inductors and the external elements comprise the input and output interdigitated capacitors.

In the first stage of the optimisation process, only the internal elements have been varied and new values for the equivalent circuit of the six inner interdigitated capacitors and seven shunt stub inductors have been computed. The purpose of this optimisation was to reduce the transmission loss ripple in the LHTL band. The optimisation was carried out using the commercial software schematic of ADS requesting minimisation of the error function (E)

$$E = \left\{ \frac{1}{K} \sum_{i=1}^{K} [|S_{21}^{ckt} - 0.5\,\text{dB}|] \right\} + |\min(f_{se}, f_{sh}) - 2.3\,\text{GHz}| \tag{10}$$

in which K denotes the number of sampled frequencies in the band and S_{21}^{ckt} is the insertion loss in dB. f_{se} and f_{sh} are the resonant frequencies of the serial and parallel resonant circuits shown in Fig. 2 and described in [3]. The error function in (10) imposes insertion loss ripple less than 0.5 dB and performance as a LHTL for frequencies less than 2.3 GHz. Once the minimum error was achieved in the first stage of the optimisation process, the input and output interdigitated capacitors were varied, while all other components of the equivalent circuit remained constant. The purpose of this optimisation was to obtain a good input match. At the end of the optimisation procedure, the components of the equivalent circuit were translated into physical dimensions of the structure using the numerical multivariable functions, and the final transmission loss

doi: 10.1049/iet-map.2010.0111

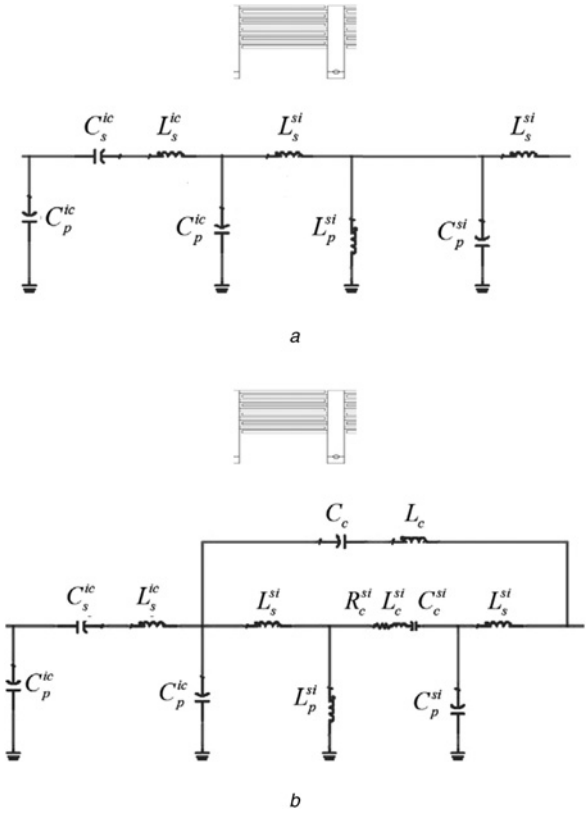

Figure 7 *Unit cell equivalent circuit of the LHTL*

a Simplified circuit model based on [4]
b Improved circuit model

performance of the LHTL was computed using the EM simulation commercial software momentum of ADS from Agilent. Comparison of the simulated results obtained based on the equivalent circuit model using ADS with the EM simulated results have shown unsatisfactory agreement indicating that the equivalent circuit [4] used to represent the LHTL is inaccurate. Consequently, an improved equivalent circuit, which takes into consideration the external coupling through radiation of the interdigitated capacitors and the coupling between the stub inductor and the interdigitated capacitors on its both sides, has been considered. Fig. 7 shows the simple and improved equivalent circuits. The capacitor and inductor (C_c, L_c), respectively, represent the external coupling between adjacent interdigitated capacitors and the resistor, capacitance and inductor (R_c^{si}, C_c^{si}, L_c^{si}), respectively, represent the coupling between the stub inductor and its adjacent interdigitated capacitors. The physical and circuit modelling parameters obtained throughout the optimisation process at different stages (initial, after internal elements optimisation and after optimisation of the in/out interdigitated capacitors) are presented in Tables 1 and 2. The computed parameters of the equivalent circuit (shown in Fig. 7*b*) of the model presented in [4] have been used as initial parameters for the optimisation process.

Fig. 8 shows the comparison between simulation results of the lumped element model of the simplistic (see Fig. 7*a*) and improved (see Fig. 7*b*) equivalent circuits using ADS circuit analysis software and the simulation results obtained based on EM simulation with momentum of ADS software after the optimisation of the internal section and after optimisation of the input and output interdigitated capacitors. One can observe a better agreement between the S_{21}[dB] computed

Table 1 Physical parameters of the circuit: before optimisation, after optimisation of the internal section and after optimisation of the input and output interdigitated capacitors

Physical parameters				Design phase
l, mm	w_f, mm	s, mm	N	
6.32	0.3	0.2	5	initial values
5	0.45	0.3	5	after internal elements optimisation
N/A	0.2	0.15	7	after in/out elements optimisation

Others parameters in the final design are $d = 0.66$ mm, $l_v = 1.47$ mm, $w_s = 0.98$ mm, $\varepsilon_r = 2.2$, $h = 1.57$ mm, $l_f = 0.99$ mm and $w_i = 2Nw_f + s(2N - 1)$

Table 2 Circuit modelling parameters: before optimisation, after optimisation of the internal section and after optimisation of the input and output interdigitated capacitors

Design phase	Lumped elements values										
	C_p^{ic}, pF	C_s^{ic}, pF	L_s^{ic}, nH	L_p^{si}, nH	C_p^{si}, pF	L_s^{si}, nH	C_c, pF	L_c, nH	R_c^{si}, Ω	L_c^{si}, nH	C_c^{si}, pF
initial value	0.545	1.41	3.298	2.48	0.308	0.14	30	0.33	7.26	1.24	10
after internal elements optimisation	0.618	1.24	2.86	2.815	0.282	0.157	11.96	0.67	8.57	2.11	3.2
after in/out elements optimisation	0.502	2.03	3.12	N/A	N/A	N/A	31.65	0.2	0.02	0.37	90.41

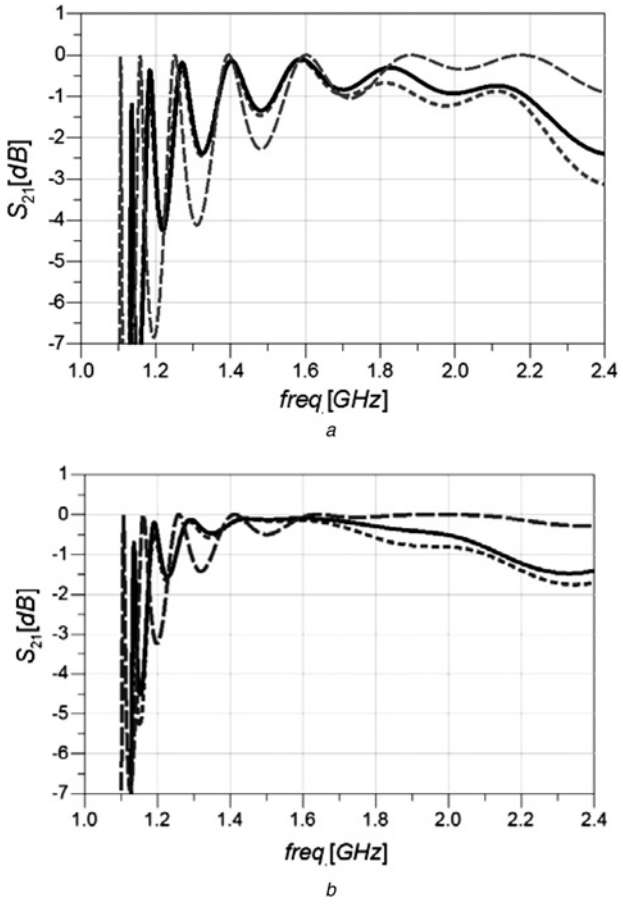

Figure 8 *Comparison between S21[dB] simulation results based on equivalent circuit modelling using schematic of ADS and EM simulation results using momentum of ADS (solid lines)*

a After optimisation of the internal section based on simple schematic of ADS modelling (dashed lines), and improved schematic of ADS modelling (dotted lines)

b After optimisation of the input and output interdigitated capacitors based on simple schematic of ADS modelling (dashed lines) and improved schematic of ADS modelling (dotted lines)

results based on the improved circuit model and the EM simulation results. In addition, a significant improvement in the S_{21}[dB] smoothness and absolute value after the optimisation process of both internal and external sections of the LHTL are also observed. Fig. 9 shows the comparison between the return loss simulation results obtained based on schematics and momentum software of ADS. The results show a good matching (better than 17 dB return loss) in the frequency band $1.4\ \text{GHz} < f < 2\ \text{GHz}$ and an improvement in the similarity between the simulated results based on the improved circuit model and the EM simulations. Table 3 shows the computation time breakdown for the various design phases of the numerical optimisation technique. The total time required is 27.7 h, from which 98% is dedicated for the data bank creation. In comparison, the computational time required for the circuit modelling and

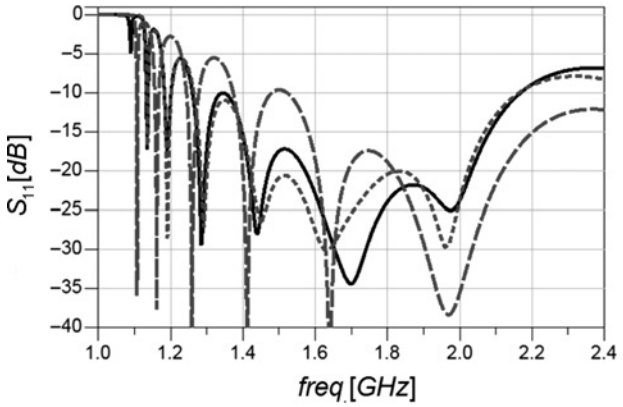

Figure 9 *Return loss simulation results obtained based on schematic of ADS (solid lines) and momentum of ADS (dotted lines) after optimisation*

Table 3 Computation time breakdown using the numerical optimisation technique

Design phase	Time per iteration, min	Number of iterations	Total time, min
EM simulation of IC for the data bank	21.2	72	1526.4
EM simulation of SI for the data bank	6	18	108
polynomial fit to EM simulation results	0.17	90	15
optimisation of the internal structure with ADS	0.55	12	6.56
optimisation of the external IC'S with ADS	0.55	12	6.56

optimisation with the physical optimisation technique was 139.5 s. The drawback of this technique is that the primitive structures are not available always with known equivalent circuits and analytical parameterisation functions to describe the device.

4 Measurements

For validation purposes, three LHTL prototypes have been fabricated: one based on the geometrical dimensions described in [4], one with the dimensions obtained after

doi: 10.1049/iet-map.2010.0111

optimisation of the internal structure and one with the dimensions after optimisation of the input and output interdigitated capacitors. The substrate used is Rogers RT/Duroid 5880 with dielectric constant $\varepsilon_r = 2.2$, loss factor $\tan\delta = 0.0009$ and thickness $h = 1.57$ mm.

A photograph of the fabricated prototypes is shown in Fig. 10. The fabricated dimensions of the internal interdigitated capacitors are $w_f = 0.45$ mm, $l_f = 9.9$ mm, $s = 0.3$ mm and $N = 5$. The dimensions of the input/output interdigitated capacitors are $w_f = 0.2$ mm, $l_f = 9.9$ mm, $s = 0.15$ mm and $N = 7$, and the dimensions of the shunt stub inductors are $l = 5$ mm, $w_s = 1.98$ mm, $d = 0.66$ mm and $w_i = 2Nw_f + s(2N - 1)$.

Comparison between the EM simulated and measured results on the prototype after optimisation of the internal structure and on the prototype after optimisation of the input and output interdigitated capacitors is shown in Fig. 11. One can observe a satisfactory agreement between the simulated and measured results and successful smoothing of the transmission loss ripples in the final prototype. A possible cause of the disagreement between the measured and simulated results could be imperfect match of the input and output connectors of the prototypes. Moreover, the undesirable notch in S_{21}[dB] behaviour is due to excitation of internal resonances caused by higher order modes.

Fig. 12 shows the measured insertion phase of the LHTL as a function of the number of unit cells for different frequencies. One can observe that for $f < 2.4$ GHz the insertion phase is positive, which is an indication that the transmission line is performing as an LHTL, for 2.4 GHz $< f <$ 2.6 GHz the insertion phase is almost zero and for $f > 2.6$ GHz the insertion phase is negative, which is an indication that the transmission line is performing as an RHTL. This feature is important in serial-fed antenna arrays, such that a combination of an LHTL and RHTL connected in tandem can be used to generate 'zero phase' feed network with low loss between two interconnected elements. To demonstrate this effect, two patches spaced

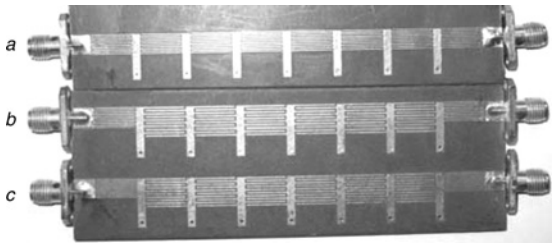

Figure 10 *Prototypes prepared for this study*

a Prototype based on data from [4]
b Prototype after optimisation of the internal structure
c Prototype after final optimisation of the input and output interdigitated capacitors

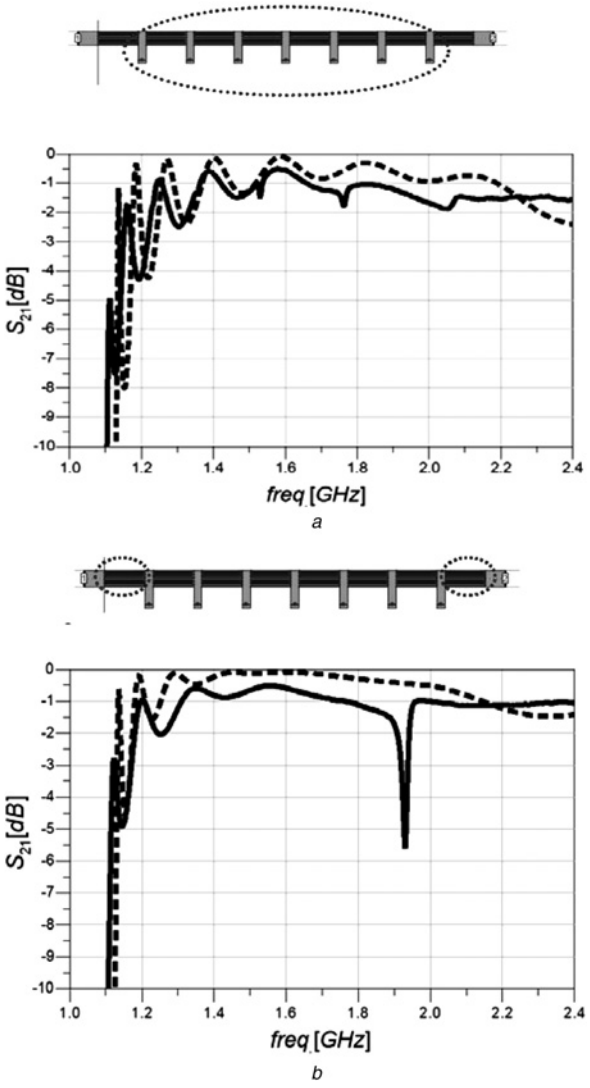

Figure 11 *Comparison between measured (solid lines) and EM simulated (dotted lines) results*

a Prototype after optimisation of the internal structure
b Prototype after optimisation of the input and output interdigitated capacitors

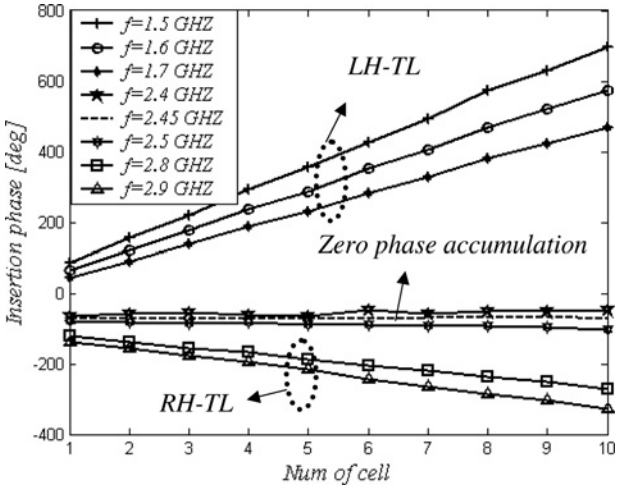

Figure 12 *Measured insertion phase along the transmission line as a function of the number of unit cells for different frequencies*

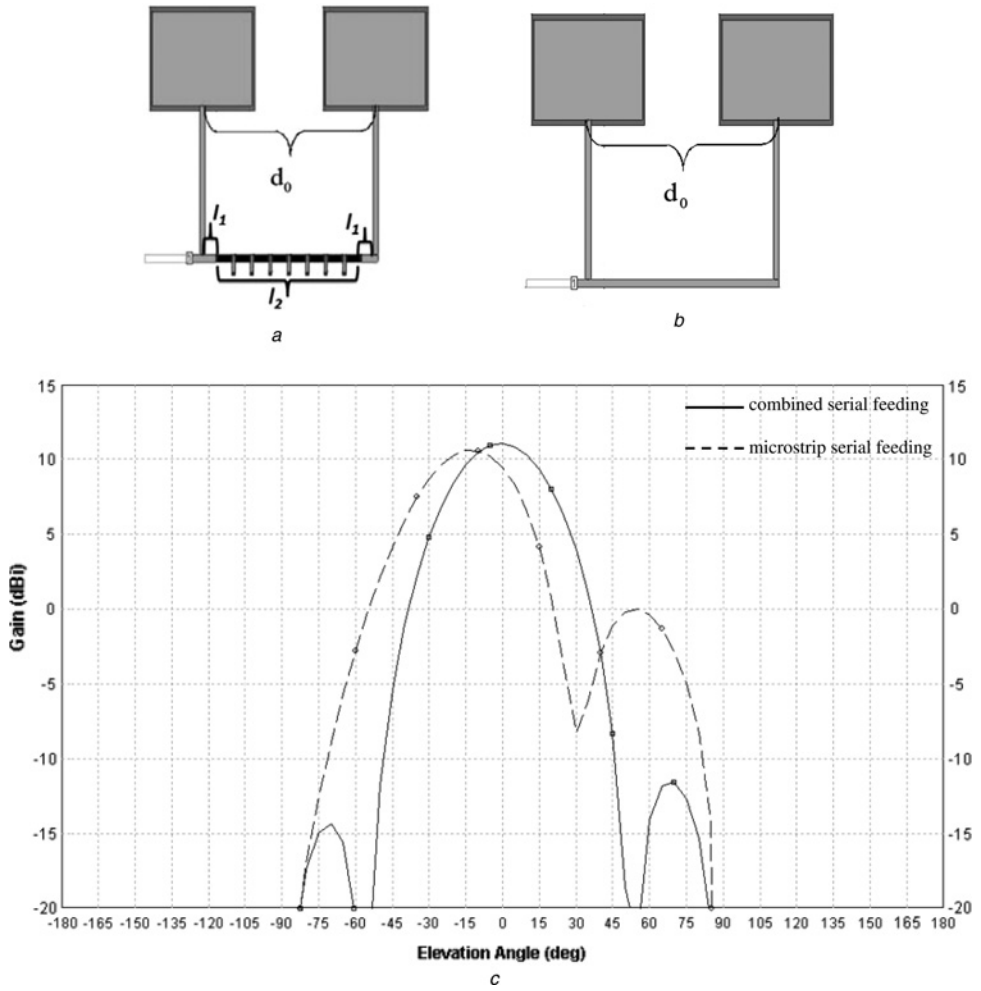

Figure 13 *Comparison between two serial feeding networks*

a Two-element patch array with a combined serial feed network (LHTL and RHTL)
b Two-element patch array with an RHTL (microstrip line) serial feed network
c Simulated H-plane radiation patterns at 1.6 GHz of the two-array geometries in *a* and *b*

$0.609\lambda_0$ at 1.6 GHz were serially connected with two different serial feed networks. One is made from a combination of an LHTL made up of seven unit cells with a total length of $l_2 = 98.9$ mm and an RHTL (standard microstrip line) with a total length of $2l_1 = 15.3$ mm and the other is made of a microstrip line with a total length of $d_0 = 114.2$ mm. Fig. 13 shows the comparison between the radiation patterns of the two elements array with the different serial feed networks. Based on Fig. 12, one can observe that in the 'zero phase' feed network, the LHTL introduces an insertion phase of $+406^\circ$, whereas the RHTL introduces an insertion phase of -46°, which totals in a 360° as required for an in-phase summation of the two-element array. On the other hand, the standard RHTL microstrip line with the same length introduces an insertion phase of -317°. The effective dielectric constant of the microstrip line is 1.86. As expected, the maximum radiation with the 'zero phase' feed network points to broadside, while in the case of the standard RHTL microstrip line feed network, the maximum radiation occurs at -15°.

5 Conclusions

Two methods for circuit modelling of an LHTL have been presented. The circuit modelling enables a more efficient way to optimise a multivariable complex structure like the LHTL vis-à-vis direct optimisation of its geometrical parameters. The objective of the circuit modelling is to obtain the equivalent circuit of the structure and determine its multivariable components functions with the physical dimensions as their variables. The first method presented is based on numerical parameterisation of the components in the equivalent circuit of the LHTL and the second method is based on integration of partial circuit physical models of the LHTL to obtain the equivalent circuit and their analytical parameterisation functions. The first method is relatively simple to implement and only needs a priori knowledge of the equivalent circuit schematics, which can be determined by physical insight. The second method was found to be more effective computationally. Comparison between the components obtained by both methods is in close agreement. A novel and improved

doi: 10.1049/iet-map.2010.0111

circuit model taking into consideration the external mutual coupling between the elements of the LHTL was used to optimise its performance in terms of absolute transmission loss and minimum ripple over a wide frequency range. The optimisation was done in two steps: first optimisation of the internal structure and second by optimisation of the input and output interdigitated capacitors. The optimised structure was simulated electromagnetically and the results found to be in good agreement with the simulation results based on circuit modelling in terms of transmission loss. Three prototypes of the LHTL representing various steps through the optimisation process have been fabricated and tested. The measurement and simulation results were compared and the agreement is satisfactory.

6 References

[1] GIL M., BONACHE J., GIL I., GARCÍA-GARCÍA J., MARTÍN F.: 'On the transmission of left-handed microstrip lines implemented by complementary split ring resonators', *Int. J. Numer. Model: Electron. Netw. Devices Fields*, 2006, **19**, (2), pp. 87–103

[2] LEVY A., SHAVIT R., HABIB L.: 'Circuit modeling and optimization of a microstrip left handed transmission line for antenna applications'. IEEE AP-S Int. Symp., San-Diego, California, 2008, pp. 268–272

[3] CALOZ C., ITOH T.: 'Electromagnetic metamaterials' (Wiley, 2006)

[4] CALOZ C., ITOH T.: 'Transmission line approach of left-handed (LH) materials and microstrip implementation of an artificial LH transmission line', *IEEE Trans.*, 2004, **AP-52**, pp. 1159–1166

[5] BANDLER J.W., CHEN S.H., IIAIJAVAD S.: 'Microwave device modeling using efficient l1 optimization: a novel approach', *IEEE Trans.*, 1986, **MTT-34**, pp. 1282–1293

[6] POZAR D.M.: 'Microwave engineering' (Wiley, 2004, 3rd edn.)

[7] BAHL I., BHARTIA P.: 'Microwave solid state circuit design' (Wiley, 2003)

[8] BENEDEK P., SILVESTER P.: 'Equivalent capacitances for microstrip gaps and steps', *IEEE Trans.*, 1972, **MTT-20**, pp. 729–733

[9] GARG R., BAHL I.J.: 'Characteristics of coupled microstrip lines', *IEEE Trans.*, 1979, **MTT-27**, pp. 700–705

[10] WADELL B.C.: 'Transmission line design handbook' (Artech House, 1991)

[11] KOMPA G.: 'Practical microstrip design and applications' (Artech House, 2005)

[12] HAMMERSTAD E.O.: 'Equations for microstrip circuit design'. European Microwave Conf., Hamburg, 1975, pp. 268–272

[13] HARRINGTON R.F.: 'Time-harmonic electromagnetic fields' (McGraw-Hill, 1961)

doi: 10.1049/iet-map.2010.0111